Radiology

Diffusion and Intravoxel Incoherent Motion MR Imaging–based Virtual Elastography: A Hypothesis-generating Study in the Liver[1]

Denis Le Bihan, MD, PhD
Shintaro Ichikawa, MD, PhD
Utaroh Motosugi, MD, PhD

Purpose: To investigate the potential of diffusion magnetic resonance (MR) imaging to provide quantitative estimates of tissue stiffness without using mechanical vibrations in patients with chronic liver diseases and to generate a new elasticity-driven intravoxel incoherent motion (IVIM) contrast.

Materials and Methods: This retrospective study, conducted from January to April 2016, was approved by an institutional review board that waived the requirement for informed consent. Fifteen subjects were included (13 men and two women; mean age ± standard deviation, 73 years ± 8). MR elastography and diffusion MR imaging were performed at 3 T. A search for an empirical relationship between MR elastographic shear modulus, μ_{MRE}, and a shifted apparent diffusion coefficient (sADC) was performed. The sADC was then inverted to estimate patient liver shear modulus directly from diffusion MR imaging signals.

Results: A significant correlation ($r^2 = 0.90$, $P = 1 \cdot 10^{-7}$) was observed between μ_{MRE} and sADC calculated by using diffusion MR imaging signals acquired with *b* values of 200 (S_{200}) and 1500 (S_{1500}) sec/mm^2 ($sACD_{200-1500}$). On the basis of the relationship between the μ_{MRE} and $sADC_{200-1500}$, a diffusion-based shear modulus, μ_{diff}, could be estimated with the following equation: $\mu_{diff} = (-9.8 \pm 0.8) \ln(S_{200}/S_{1500}) + (14.0 \pm 0.9)$. IVIM virtual elastograms also could be generated to reveal new contrast features in lesions, depending on pseudovibration frequency and amplitude.

Conclusion: Diffusion MR imaging, through a calibration of $sADC_{200-1500}$ with standard MR elastography, can be converted quantitatively into shear modulus without using mechanical vibrations to provide information on the degree of liver fibrosis; these virtual elastograms require only two *b* values to be acquired and processed. Propagating shear wave can also be emulated, leading to a new elasticity-driven IVIM contrast with ranges of virtual vibration frequencies and amplitudes not limited by MR elastography or MR imaging hardware capacities.

Online supplemental material is available for this article.

[1] From Neurospin, Bât 145, CEA-Saclay Center, Gif-sur-Yvette 91191, France (D.L.B.); Department of Radiology, Kyoto University Graduate School of Medicine, Kyoto, Japan (D.L.B.); and Department of Radiology, University of Yamanashi, Yamanashi, Japan (S.I., U.M.). Received January 4, 2017; revision requested February 10; revision received February 14; accepted March 17; final version accepted March 23. **Address correspondence to** D.L.B. (e-mail: *denis.lebihan@gmail.com*).

D.L.B. supported by the Louis-Jeantet Foundation.

Over the past 2 decades magnetic resonance (MR) elastography has emerged as a promising approach to characterize soft tissue on the basis of its mechanical properties (1,2), and has been used successfully for liver fibrosis staging (3). MR elastography can be a noninvasive alternative to liver biopsy, the reference standard of liver fibrosis staging, but with a risk of complications including hemorrhage and infection. Also, substantial interpathologist variation is known for fibrosis staging of biopsy specimens (4).

MR elastography is reliant on three steps (1,5,6): *(a)* producing propagating shear waves in tissue, generally by using an external mechanical vibrator; *(b)* acquiring MR phase images sensitive to the tissue displacements induced by the vibration (approximately a few micrometers in amplitude) by using gradient pulses oscillating at a frequency similar to that of the the mechanical vibrations; and *(c)* processing the phase images of the propagating shear waves to transform them to tissue mechanical properties (eg, shear modulus, μ).

Although the utility of MR elastography for liver fibrosis staging has been well described (3,5), it still has some limitations. MR elastography is costly, requiring dedicated hardware and software. Beside the installation of a mechanical setup for each patient, the use of specific MR elastographic sequences adds to the patient's examination time. MR elastography is difficult to use for the tissues located deep in the body because of the fast damping of the waves' amplitude when penetrating tissues. The reverse transformation of the measured phase shifts into wavelengths is not straightforward and is subject to confounding effects.

On the other hand, diffusion MR imaging (7) has been shown to be exquisitely sensitive to tissue structure at a microscopic level (8), because diffusion of water is hindered by tissue components such as fibers or cell membranes. Diffusion MR imaging is being used for a variety of physiologic or pathologic conditions (9) and results of some studies (10,11) have shown that both MR elastography and diffusion MR imaging have clinical value in staging of hepatic fibrosis. However, authors of previous studies (11,12) generally have concluded that MR elastography slightly outperforms diffusion MR imaging assessment of liver fibrosis. The results of one study (13) also suggest that the acquisition of diffusion MR imaging and MR elastographic images might be combined in a single MR imaging sequence. However, authors of those studies stopped short of suggesting that diffusion MR imaging and MR elastography might, indeed, reflect common mechanistic tissue features.

Hypothesizing that there might be a strong relationship between tissue water diffusivity and tissue elastic properties, we investigated the potential of diffusion MR imaging to provide quantitative estimates of tissue stiffness without using mechanical vibrations in patients with chronic liver diseases and to generate a new elasticity-driven intravoxel incoherent motion (IVIM) contrast.

Advances in Knowledge

- There was a significant correlation ($r^2 = 0.90$, $P = 1 \cdot 10^{-7}$) in the liver between standard MR elastographic shear modulus and a shifted apparent diffusion coefficient calculated from diffusion MR imaging signals acquired with *b* values of 200 and 1500 sec/mm^2, a biomarker of Gaussian and non-Gaussian diffusion.
- After suitable calibration of the shifted apparent diffusion coefficient with the stiffness value measured by means of standard MR elastography, liver tissue shear modulus can be estimated directly from diffusion MR imaging signals acquired with *b* values of 200 and 1500 sec/mm^2.
- Intravoxel incoherent motion virtual elastograms of the liver can be emulated for a wide range of pseudovibration frequencies and amplitudes without using mechanical vibrations.

Implications for Patient Care

- Staging of liver fibrosis could be performed with non-Gaussian diffusion MR imaging with the same accuracy as that of standard MR elastography.
- Virtual elastograms of the liver can be emulated by using intravoxel incoherent motion diffusion MR imaging without using mechanical vibrations.

Materials and Methods

Patient Population

This retrospective study conducted from January to April 2016 was performed in accordance with the principles of the Declaration of Helsinki and was approved by an institutional review board that waived the requirement for informed consent. Twenty-three consecutive patients with diagnoses of chronic liver diseases initially were included. Eight patients were excluded because of artifacts on MR elastographic or diffusion MR images (mainly from respiratory or heart motion). Hence, this part of

https://doi.org/10.1148/radiol.2017170025

Content code: GI MR

Radiology 2017; 285:609–619

Abbreviations:
ADC = apparent diffusion coefficient
IVIM = intravoxel incoherent motion
NGD = non-Gaussian diffusion index
sADC = shifted ADC

Author contributions:
Guarantor of integrity of entire study, D.L.B.; study concepts/study design or data acquisition or data analysis/interpretation, all authors; manuscript drafting or manuscript revision for important intellectual content, all authors; approval of final version of submitted manuscript, all authors; agrees to ensure any questions related to the work are appropriately resolved, all authors; literature research, D.L.B., S.I.; clinical studies, S.I., U.M.; experimental studies, D.L.B.; statistical analysis, D.L.B.; and manuscript editing, D.L.B., U.M.

Conflicts of interest are listed at the end of this article.

Table 1

Patient Data with Results of Standard MR Elastography and Diffusion MR Imaging–based Virtual MR Elastography

Age	Sex	ALT Level (U/L)	Diagnosis	MR Elastography Shear Modulus (kPa)	Diffusion MR Imaging Virtual Shear Modulus (kPa)	$sADC_{200-1500}$ ($10^{-3}mm^2/sec$)	ADC_{0-1000} ($10^{-3}mm^2/sec$)
67	M	18	Hepatitis B virus	2.6 ± 0.2	2.6 ± 1.5	0.89 ± 0.15	1.23 ± 0.13
72	M	84	Hepatitis C virus	6.3 ± 0.6	6.1 ± 0.9	0.62 ± 0.09	0.95 ± 0.08
72	M	29	Nonalcoholic steatohepatitis	3.5 ± 0.3	3.6 ± 0.5	0.82 ± 0.05	0.99 ± 0.04
78	M	80	Hepatitis C virus	5.1 ± 0.4	5.3 ± 0.6	0.69 ± 0.06	0.90 ± 0.06
81	M	14	Hepatitis C virus	3.7 ± 0.2	3.0 ± 0.7	0.86 ± 0.07	1.14 ± 0.06
65	M	35	Hepatitis B virus	3.7 ± 0.5	3.8 ± 0.8	0.80 ± 0.09	1.03 ± 0.08
84	F	56	Hepatitis C virus	4.6 ± 0.6	4.7 ± 0.7	0.73 ± 0.07	0.93 ± 0.06
66	M	29	Hepatitis C virus	2 ± 0.3	2.0 ± 0.8	0.94 ± 0.08	1.18 ± 0.07
73	M	21	Hepatitis B virus	2.6 ± 0.3	2.9 ± 1.3	0.87 ± 0.13	1.15 ± 0.12
60	M	58	Nonalcoholic steatohepatitis	4.2 ± 0.3	4.5 ± 1.9	0.74 ± 0.20	1.17 ± 0.17
78	M	10	. . .	1.9 ± 0.2	1.2 ± 0.7	1.01 ± 0.07	1.30 ± 0.06
83	M	44	Hepatitis C virus	3.8 ± 0.4	3.3 ± 0.9	0.84 ± 0.09	1.05 ± 0.08
63	M	39	. . .	3 ± 0.4	2.7 ± 0.7	0.89 ± 0.07	1.24 ± 0.06
80	F	15	Hepatitis C virus	3.1 ± 0.3	3.5 ± 0.7	0.82 ± 0.07	1.14 ± 0.06
77	M	29	Hepatitis C virus	3.2 ± 0.3	4.0 ± 1.2	0.79 ± 0.13	1.05 ± 0.11

Note.—ALT = alanine aminotransferase.

the study was finally performed with 15 patients. Study subjects included 13 men and two women (mean age, 73 years ± 8; range, 60–84 years; mean age for men, 72 years; range, 60–83 years; mean age for women, 82 years; range, 80–84 years) (Table 1). Fibrosis stage (METAVIR scoring system) was estimated from MR elastographic findings by using cutoff values previously described (14). The causes of chronic liver disease included hepatitis C virus (n = 8), hepatitis B virus (n = 3), and nonalcoholic steatohepatitis (n = 2); in two patients there was no underlying hepatitis. Five patients also presented with small tumors (hepatic carcinoma and metastases). Serum alanine aminotransferase, or ALT, levels were obtained from blood samples collected within 1 week of the MR imaging examinations.

MR Imaging Data Acquisition and Processing

Patients were examined with a 3-T MR imager (Discovery 750; GE Medical Systems, Milwaukee, Wis) with a 32-channel phased-array coil.

MR elastography.—For MR elastography, external vibration (60 Hz) to the liver was induced from a passive driver linked to a vibrator and positioned on the right chest wall of the patient in a supine position. A vibrator placed outside the imaging room produced a pneumatic vibration that was delivered to the passive driver by means of a plastic cylinder (Mayo Clinic, Rochester, Minn) (15). MR elastography was performed with a two-dimensional gradient-echo sequence on the axial plane, which was set from above the gallbladder to below the subphrenic region of the liver. For acquiring images in consistent positions at each phase offset, the patients were asked to hold their breath after expiration. Acquisition parameters were: repetition time msec/echo time msec, 50/20; flip angle, 23°; number of signals acquired, one; matrix, 256 × 80; section thickness, 5 mm; field of view, 40 × 40 cm^2; with motion-sensitizing gradient along the z axis. Stiffness maps were calculated by using a two-dimensional inversion algorithm implemented in the imager (6) and liver shear modulus was estimated from regions of interest on the stiffness maps. Care was given to locate regions of interest away from large vessels and tumors in the patients with carcinoma.

Diffusion MR imaging.—For diffusion MR imaging, a fat-suppressed spin-echo echo-planar sequence was used with the following parameters: 4000/56.6; respiratory gating in the expiratory phase; number of signals acquired, two; section thickness, 4 mm; matrix, 100 × 100; and field of view, 40 × 40 cm^2. Images were acquired with diffusion encoding along the x, y, and z axes with 14 b values between 0 and 1500 sec/mm^2, but only 0, 200, 400, 600, 1000, 1200, and 1500 sec/mm^2 b values were considered for this study.

A shifted apparent diffusion coefficient (sADC) was calculated by using two key b values(low key b value, LKb, and high key b value, HKb) optimized to reflect Gaussian and non-Gaussian diffusion (Appendix E1 [online]) as:

$$sADC = \ln\left(S_{LKb}/S_{HKb}\right)/(HKb - LKb) \quad (1),$$

where S_{LKb} and S_{HKb} are intensities of the signals acquired at the low and high key b values, respectively. Results of a previous analysis suggested that 200 and 1500 sec/mm^2 is the best combination (Appendix E1 [online]), but other combinations of LKb and HKb were also tested (LKb = 0, 200 and 400 sec/mm^2; HKb = 600, 1000, 1200, 1500

Figure 1

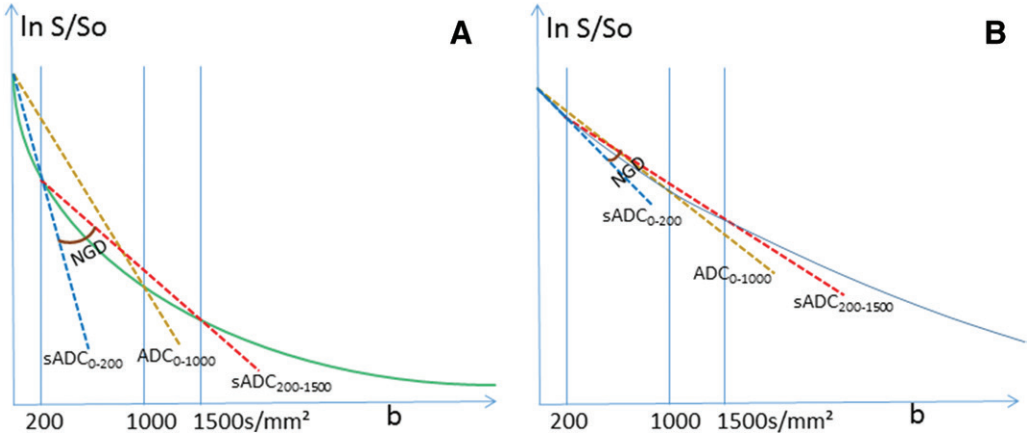

Figure 1: Graphs show effects of non-Gaussian diffusion on diffusion MR imaging signal. In the presence of non-Gaussian diffusion, the plot of the logarithm of the diffusion signal aquired for each *b* value is not a straight line but curved, especially at high *b* values. Non-Gaussian diffusion has clinical potential because it reflects interaction of water molecules with tissue elements, mainly cell membranes. To increase weighting of non-Gaussian diffusion to the standard ADC (calculated from *b* values of 0 and 1000 sec/mm^2) one may switch to an sADC by using higher *b* values (eg, 200 and 1500 sec/mm^2). *B*, While ADC and $sADC_{200–1500}$ are similar in the presence of weak non-Gaussian diffusion, *A*, the $sADC_{200–1500}$ becomes much smaller than the ADC with large non-Gaussian diffusion effects. Non-Gaussian diffusion effects can be quantified by using an NGD, reflecting the angle between sADC values obtained with low (eg, 0 and 200 sec/mm^2) and high *b* values. Graphs were generated by using synthetic (noiseless) data to provide an enhanced display of the non-Gaussian diffusion features. *S* = signal intensity at each *b* value, *So* = signal intensity at *b* = 0.

sec/mm^2). The sADC calculated by using the pair of 0 and 1000 sec/mm^2, is the standard ADC.

A non-Gaussian diffusion index (NGD) was also calculated and defined as:

$$NGD = 6\{\ln(S_0/S_{LKb})/LKb - \ln(S_{LKb}/S_{HKb})/(HKb - LKb)\}/\{HKb[\ln(S_0/S_{LKb})/LKb]^2\} \quad (2),$$

where S_0 is the signal intensity obtained for $b = 0$. For the three key b values used in this study (0, 200, and 1500 sec/mm^2) NGD reduces to:

$$NGD = 6(sADC_{0–200} - sADC_{200–1500})/(1500\ sADC_{0–200}{}^2) \quad (3).$$

Basically, this index is a normalized comparison of the slopes of the diffusion MR imaging signal intensity attenuation with *b* values between 0 and 200 sec/mm^2, and *b* values between 200 and 1500 sec/mm^2, respectively. If diffusion is truly Gaussian (free) both slopes are identical and NGD equals 0. In the presence of non-Gaussian diffusion, the slope at high *b* values is less than that at low *b* values (Fig 1) and NGD increases with the amount of deviation from Gaussian diffusion. This index has the advantage of providing information on non-Gaussian diffusion from signals acquired at only three key *b* values, avoiding complex signal modeling with a large number of *b* values. It can be shown that if the low key *b* value is low enough so that non-Gaussian diffusion effects can be neglected, NGD is formally equal to the kurtosis parameter of the kurtosis model (16,17) in the absence of blood IVIM effects (Fig 1) (perfusion-related IVIM effects, through an increase of the slope at low *b* values, also contributes to NGD). Data were processed in a voxel-by-voxel analysis and regions of interest were placed in the liver by a reader (D.L.B., with 30 years of experience) who was blinded to the MR elastographic results, avoiding the tumors in the patients with carcinoma.

Diffusion and IVIM Virtual MR Elastography

Estimating tissue shear modulus from diffusion MR imaging.—After identifying which key *b* value combination led to the highest correlation between the sADC and MR elastographic shear modulus, μ_{MRE}, we searched for an empirical functional relationship between sADC and μ_{MRE} from the scattered plots of sADC and μ_{MRE} by using data from the first seven patients as a calibration step. The validity of this relationship was then verified by including data from the remaining eight patients.

Inverting this relationship, diffusionbased tissue shear modulus, μ_{diff}, could then be estimated from the sADC obtained with those key *b* values, or more directly from the signal intensity attenuation, S_{LKb}/S_{HKb}, as:

$$\mu_{diff} = g[\ln(S_{LKb}/S_{HKb})] \quad (4).$$

μ_{diff} was obtained on a region-of-interest basis or on a voxel-by-voxel basis

Figure 2

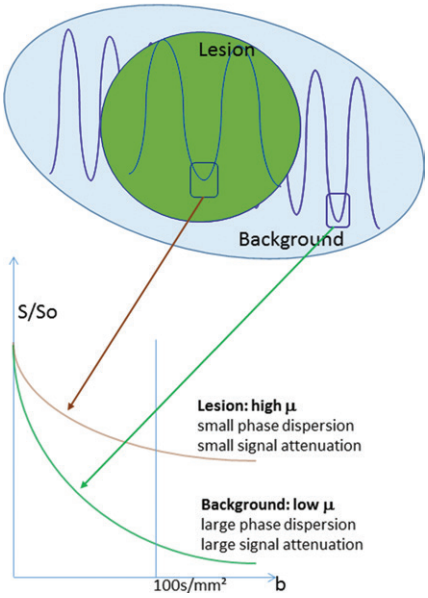

Figure 2: Illustration shows principle of IVIM elastography. Shear waves propagating through tissues result in small tissue displacements perpendicular to the propagation direction. The wavelength depends on underlying tissue elasticity: Hard tissues have longer wavelengths than do soft tissues. In the presence of oscillating motion probing gradient pulses, wavelength is estimated from signal phase associated with tissue displacements with standard MR elastography. However, phase dispersion present in each voxel also leads to reduction of signal amplitude (IVIM-like effect) that depends on the motion-probing gradient strength (*b* value) and the wavelength, hence the tissue elasticity: Hard tissues (such as lesions) are less attenuating than are soft tissues (such as organ background), creating an interesting contrast. *S* = signal intensity at each *b* value, *So* = signal intensity at *b* = 0, μ = shear modulus.

to generate three-dimensional virtual shear stiffness maps by using in-house software (Matlab R2016a; Mathworks, Natick, Mass).

Data statistical analysis.—Correlation between diffusion MR imaging and MR elastographic data were quantified by using Pearson correlation coefficient's square calculated by using software Matlab (Mathworks). After finding out that the relationship between $sADC_{200-1500}$ and MR elastographic shear modulus looked linear, we performed a linear regression analysis to get the parameters of the relationship. *P* values smaller than .05 were considered to indicate a significant difference.

Elasticity-driven IVIM contrast.—In a further step, those stiffness maps were then used to emulate contrast, which would result from the simulated microscopic motion induced by virtual propagation of shear waves through the tissue. Such motion, if real, would result in the presence of motion-encoding gradients in an intravoxel phase dispersion and a signal intensity attenuation (Fig 2). This is, by definition, an IVIM effect (7), although in this case, it is not related to the perfusion with which the IVIM concept is often associated. The degree of attenuation in those IVIM images depends on the tissue elasticity and on the choice of acquisition parameters (mainly IVIM *b* value, vibration frequency, and amplitude of the propagating shear waves) (Appendix E2 [online]). Here, we emulate those IVIM images by simulating the intravoxel phase dispersion that would result from virtual propagating waves of any amplitude and frequency by using the elasticity (μ_{diff}) maps obtained with diffusion MR imaging. The virtual parameters used for this emulation, especially key *b* values, are not to be confounded with the (real) diffusion MR imaging parameters used to estimate μ_{diff}. Considering that tumors or fibrosis generally have a larger shear modulus than do normal tissue, one may find a suitable frequency range for the shear wave and a range of virtual acquisition parameters that will highly reduce the signal in the normal tissue, while only slightly reducing the signal in the lesion or parts of the lesions, making them highly visible based on their shear stiffness. This elasticity-driven virtual IVIM contrast concept was tested in the patients with liver tumors by using pseudovibration frequencies ranging from 50 HZ to150 Hz. The overall processing flowchart for standard MR elastography, diffusion-based MR elastography and virtual IVIM elastography is outlined in Figure 3.

Results

A significant correlation was found between the standard ADC (*b* = 0, 1000 sec/mm²) and MR elastographic shear stiffness ($r^2 = 0.62$, $P = 5.3 \cdot 10^{-3}$) in accordance with earlier results showing a relationship between ADC and fibrosis stages (10,11,18–20) (Fig 4a). There was also a moderate but significant correlation between NGD and MR elastographic shear stiffness ($r^2 = 0.50$, $P = 3 \cdot 10^{-3}$) (Fig 4b). Among the tested key *b* value combinations, the pair (200–1500 sec/mm²) gave the highest correlation, as expected (Appendix E2 [online], Table 2). The relationship between $sADC_{200-1500}$ and MR elastographic shear modulus in the first seven patients was found to be strikingly linear ($r^2 = 0.995$, $P = 8 \cdot 10^{-8}$) (Fig 4), according to the following equation: $sADC_{200-1500} = 8 \cdot 10^{-5}\,\mu_{MRE} + 1.1 \cdot 10^{-3}$. Reversing this relationship, equation 4 could then be empirically established as:

$$\mu_{diff} = \alpha \ln\left(S_{200}/S_{1500}\right) + \beta \qquad (5),$$

with $\alpha = -9.8 \pm 0.8$ and $\beta = 14.0 \pm 0.9$.

Equation 5 was then used to estimate shear stiffness for the remaining eight patients. Correlation between μ_{MRE} and μ_{diff} in those patients was significant ($r^2 = 0.80$, $P = 3 \cdot 10^{-3}$). Finally, when all 15 patients were taken into account, the correlation coefficient was $r^2 = 0.90$ ($P = 1 \cdot 10^{-7}$) (Fig 5). By using cutoff values that were previously established for MR elastography–based liver fibrosis staging (10), fibrosis stages obtained from the diffusion-based shear modulus, μ_{diff}, were in full agreement with those obtained with standard MR elastography (F1: two patients; F2: three patients; F3: six patients; F4: four patients) (Fig 5).

Color-encoded maps of shear stiffness could be generated throughout the whole liver, sharing the spatial resolution and multisection features of native diffusion MR imaging and keeping the visibility of organ features, while images obtained with standard MR elastography appeared most often featureless (Fig 6, Fig E1 [online]). In patients with tumors, three-dimensional virtual elastograms generated at various pseudovibration frequencies on the basis of

Figure 3

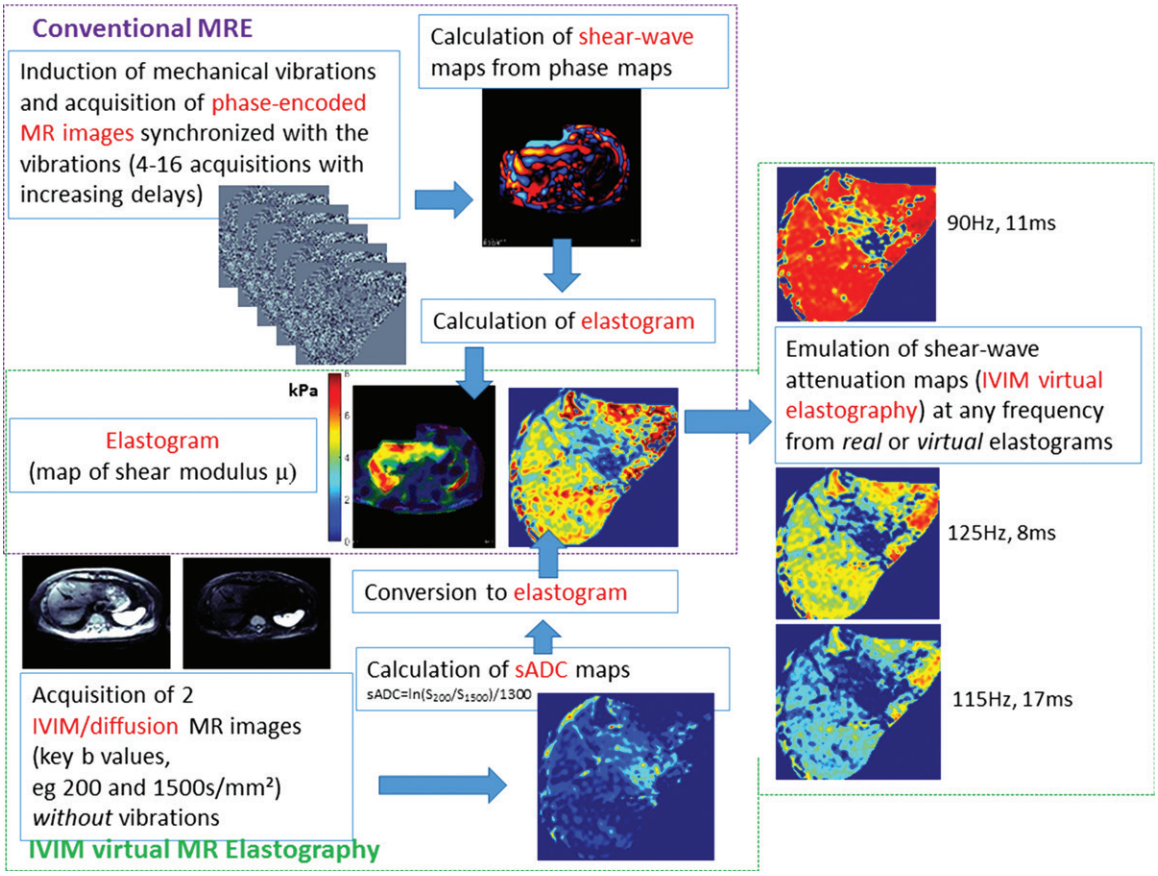

Figure 3: Illustration shows comparison of standard MR elastography and IVIM virtual elastography. With standard MR elastography, sets of phase-encoded images sensitized to induced mechanical vibrations are combined to produce shear wave maps which, in turn, can be transformed into maps of tissue elasticity (elastogram). With diffusion MR imaging virtual elastographic images at two key *b* values are acquired (without any vibration) to calculate quantitative sADC maps, which are then converted to elastograms on the basis of a calibrated relationship between sADC and tissue elasticity (shear modulus). In addition, maps of the shear modulus can be used to emulate shear wave attenuation maps through an IVIM-like effect for any virtual combination of pseudovibration amplitudes and frequencies. *MRE* = MR elastography.

equation E6 (online) revealed different contrast to allow the details within lesions to be seen, depending on the virtual frequency, that were otherwise not easily visible on the native sADC maps (Fig 7). In other words, the elasticity-driven virtual IVIM contrast acted as a postprocessing filter, enhancing or hiding lesion features according to the chosen parameters.

Discussion

If this study, we found evidence that there is a strong correlation between liver tissue elastic properties, as revealed with standard MR elastography, and tissue microstructure, as shown with diffusion MR imaging. More specifically, we found a striking linear quantitative relationship between the $sADC_{200-1500}$ and the shear modulus, μ_{MRE}, obtained from MR elastography. This strong correlation is not surprising, because elastic properties of tissues must be linked in some way to the layout of tissue elementary components (cells, fibers, stroma) to which diffusion MR imaging is exquisitely sensitive, as observed ex vivo in the intervertebral disk (18). As previously reported (10,11,19–21), we found a significant but moderate correlation of MR elastographic shear modulus with standard ADC and a significant but moderate correlation with NGD. However, the correlation between shear modulus and diffusivity was more prominent with the $sADC_{200-1500}$ in which non-Gaussian diffusion effects are incorporated over the ADC (9). Non-Gaussian diffusion occurs when molecular diffusion deviates from free diffusion, mainly because water molecules interact with tissue elements, such as cell membranes. The strong linearity of the relationship, however, cannot be explained at this stage, as there is no formal model yet to link elastic properties of tissues with their complex texture and architecture. Nonetheless, those results suggest that

Figure 4

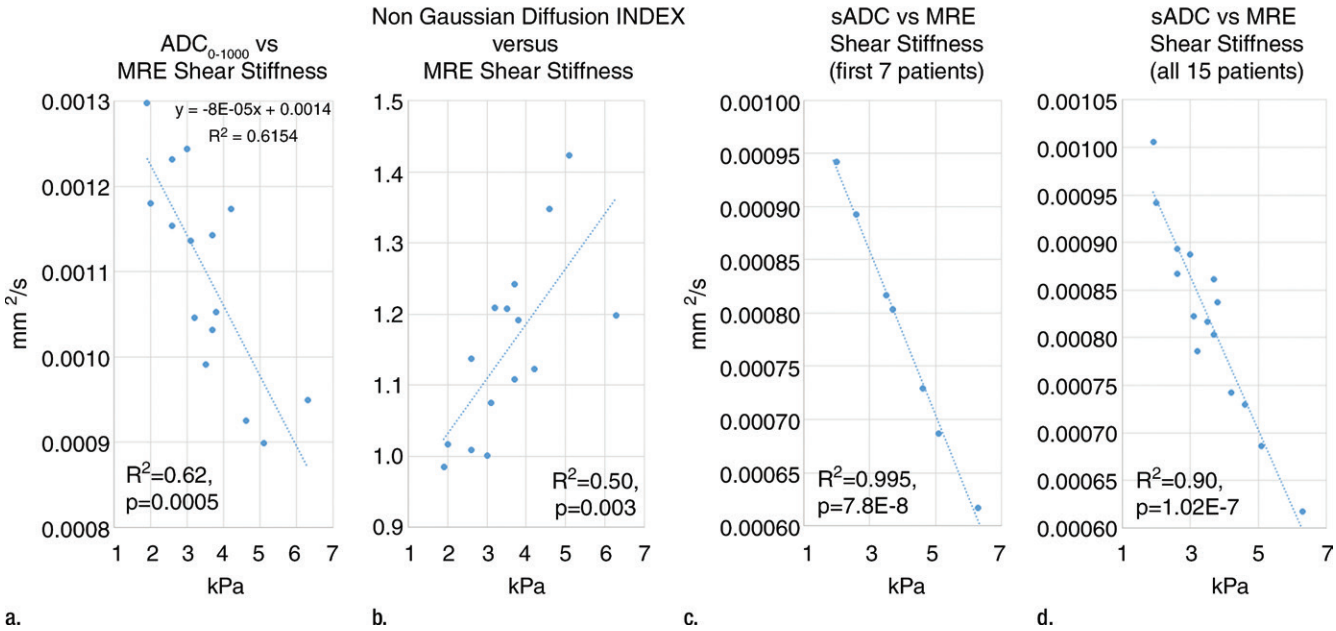

Figure 4: Graphs show correlation between diffusion MR imaging biomarkers and standard MR elastographic shear modulus. A significant but moderate correlation was found between the MR elastographic shear modulus and the standard $ADC_{0–1000}$ ($R^2 = 0.62$, $P = .0005$) and the NGD ($R^2 = 0.50$, $P = .003$). The correlation between $sADC_{200–1500}$ and MR elastographic shear modulus with the first seven patients was significant ($R^2 = 0.995$, $P = 7.8 \cdot 10^{-8}$), revealing linear relationship, confirmed when all patients were included ($R^2 = 0.90$, $P = 1.02 \cdot 10^{-7}$). *MRE* = MR elastography.

elastic properties of tissues might be derived directly and quantitatively from diffusion images acquired by using only two key *b* values, an important step considering the limitations of standard MR elastography and the flexible features available from diffusion MR imaging.

Many variants of MR elastography have been proposed, but most suffer from the burden and cost of the necessary mechanical set-up for standard MR elastography and the need for several image sets (typically four to 16) to be acquired with different phase offsets to sample the speed of the wave propagation through the tissue. Limits of the mechanical wave frequencies and the MR imaging gradient hardware also impose limits on the image spatial resolution that can be reached, often to a fraction of the native MR imaging resolution, and the range of stiffness that can be explored. High-frequency waves would allow higher spatial resolution, but with these, fast damping through the organs becomes an issue, especially in the liver, because it extends deep under the chest wall. The reverse transformation of the measured complex-valued signal phase shifts into tissue movement also is not straightforward, is subject to confounding effects (5), and sometimes results in only small portions of the imaged section to be usable.

In comparison, virtual shear modulus maps derived from the sADC intrinsically benefit from the features of diffusion MR imaging, such as multisection or full three-dimensional coverage. Acquisition of diffusion images at only two *b* values is fast, and the resulting sADC calculation is straightforward and insensitive to background phase effects. Still, diffusion MR imaging suffers from its own limitations, mainly low signal-to-noise ratios, particularly at high *b* values, and sensitivity to motion artifacts, especially in the body (eight of 23 patient data sets were rejected in our study). However, given that only two values are necessary, one might consider acquiring multiple data sets for averaging, or better, navigation algorithms to reject in real-time corrupted data sets.

Table 2

Correlation of Various ADC Combinations with MR Elastographic Shear Modulus

Correlation with MR Elastographic Shear Stiffness	r^2 Value
Standard ADC (0–1000)	0.62
$sADC_{0–600}$	0.43
$sADC_{0–1200}$	0.48
$sADC_{0–1500}$	0.67
$sADC_{200–1500}$	0.89
$sADC_{400–1500}$	0.57

Because the shear modulus obtained directly from standard MR elastography and the shear modulus that was virtually derived from sADC were very close, they led to the same estimated stages of liver fibrosis in our patient population. Indeed, pending validation in a much larger patient cohort, our results suggest that liver fibrosis might be estimated directly and accurately from the $sADC_{200–1500}$. Still, we think that elastography, real or virtual, remains a

Figure 5

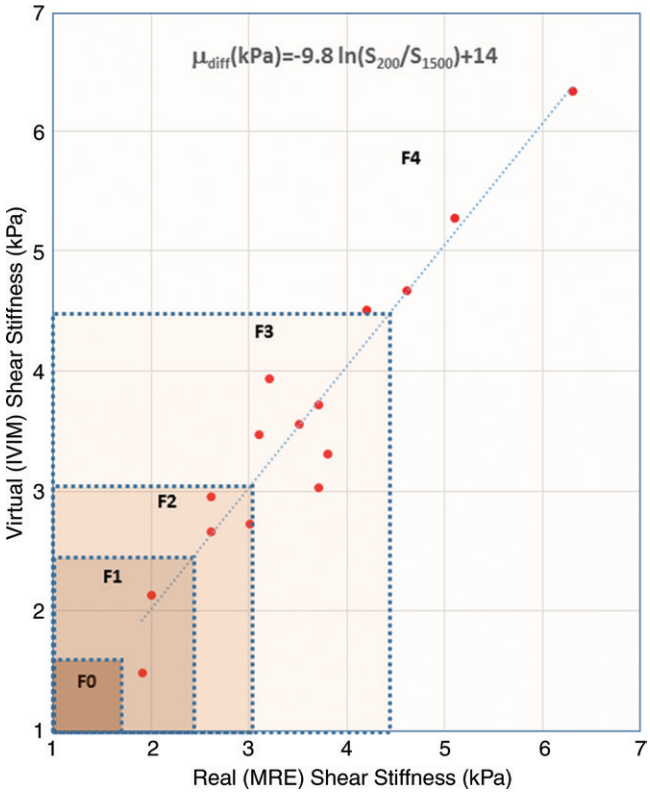

Figure 5: Graph shows comparison of virtual diffusion MR imaging–based and standard (MR elastography) shear modulus. The agreement between the shear modulus estimated from sADC, μ_{diff}, and that obtained from standard MR elastography, as well as the resulting liver fibrosis stages obtained by means of both methods on the basis of previously established cutoffs were very good. *MRE* = MR elastography.

powerful concept, because elastograms can generate clinically useful contrast not obtainable by means of other approaches, because shear modulus maps obtained either from standard MR elastography or from sADC maps could be transformed to create an interesting new elasticity-driven IVIM contrast that has not been investigated yet.

This IVIM (intravoxel phase dispersion) effect was proposed originally for estimation of tissue stiffness with real vibration (22). However, this effect highly depends on the vibration amplitude (Appendix E2 [online]), making this approach difficult to use in practice with real shear waves to estimate stiffness, because the wave amplitude varies a great deal within the organ owing to damping, and also varies among patients. However, the new IVIM virtual elastographic framework introduced in this study is different. Here, an elasticity-driven virtual IVIM contrast (IVIM virtual elastography) is emulated, in a reverse way, from the tissue elasticity maps derived from the sADC, as a postprocessing step, for any virtual shear wave propagating perfectly and homogeneously through the organ. Depending on the combination of parameters used to acquire those IVIM virtual elastograms, some tissue features might be suppressed or amplified, creating exciting contrast based on the tissue elastic properties, as shown in figure 7.

The IVIM virtual elastograms obviously do not contain any more information that the sADC maps used to generate them, but they can be considered to be advanced filtered maps that can enhance the detectability of features in lesions. A powerful feature of those IVIM virtual elastograms, however, is that they can be generated for pseudovibration frequencies and amplitudes and gradient pulse intensities that might not be technically achievable with current hardware. Because the shear modulus is known to depend slightly on the mechanical wave frequency, the shear modulus values obtained by using the 60-Hz MR elastography calibration (equation 5) might differ slightly from elasticity values obtained at another frequency, and one should remain aware that the IVIM virtual elastograms emulated at any given frequency might deviate slightly from the contrast that would be obtained at this frequency with real mechanical vibrations.

Although the results we have obtained are clear, our study should only be considered as hypothesis generating at this stage. Clearly, further validation of the relationship between the sADC and MR elastographic shear modulus with a much larger patient cohort with a wider range of abnormalities that lead to liver fibrosis (eg, alcoholic steatohepatosis, primary biliary cirrhosis, schistosomiasis, cholangitis) is needed. Other components to tissue stiffness than fibrosis may also affect both standard and virtual MR elastographic results. Indeed, inflammation, hemochromatosis, or steatosis might affect the sADC and the MR elastographic shear modulus to different degrees (12), which may lessen the strong correlation that we have observed in our series. As for other organs and diseases, especially those of the spleen (portal hypertension), breast, and prostate (cancer) or the brain (neurologic disorders), there is no reason to think that tissue elastic properties and tissue microstructure are less tightly related than are those in liver tissue. However, MR elastographic shear modulus and sADCs are different in those organs, so that the empirical relationship that might exist between those two parameters must be investigated and calibrated. This calibration step could be done,

Figure 6

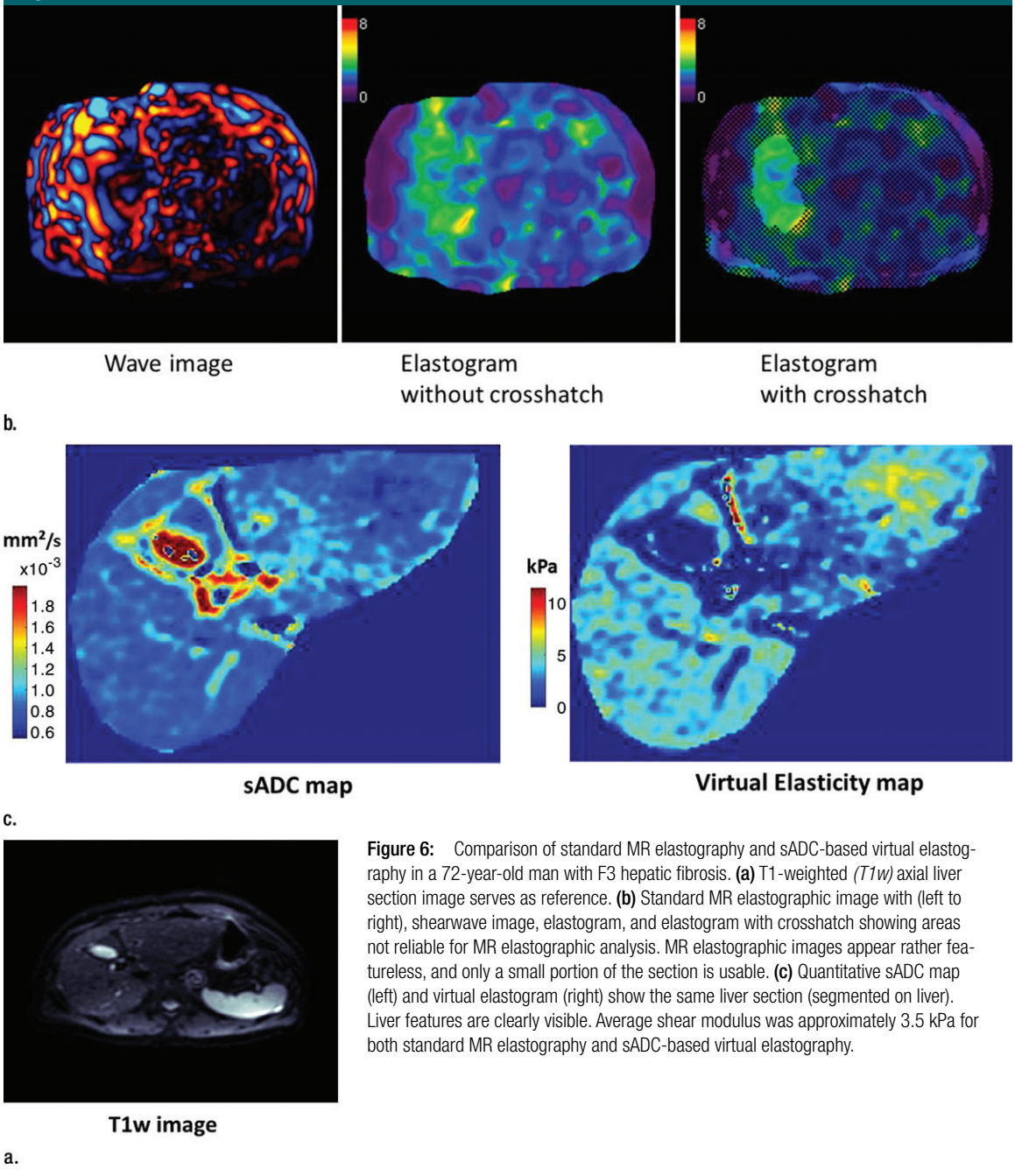

Figure 6: Comparison of standard MR elastography and sADC-based virtual elastography in a 72-year-old man with F3 hepatic fibrosis. **(a)** T1-weighted *(T1w)* axial liver section image serves as reference. **(b)** Standard MR elastographic image with (left to right), shearwave image, elastogram, and elastogram with crosshatch showing areas not reliable for MR elastographic analysis. MR elastographic images appear rather featureless, and only a small portion of the section is usable. **(c)** Quantitative sADC map (left) and virtual elastogram (right) show the same liver section (segmented on liver). Liver features are clearly visible. Average shear modulus was approximately 3.5 kPa for both standard MR elastography and sADC-based virtual elastography.

in principle, once for a given organ or abnormality, providing that the exact same diffusion MR imaging acquisition parameters are used throughout different sites and MR imagers. Standardization remains an important issue, more generally, for diffusion MR imaging applications.

Finally, diffusion-based MR elastography and IVIM virtual elastography may not give a full account of all elastic properties of tissues. Our approach might suffice in some clinical frameworks, such as in the diagnosis and staging of liver fibrosis on the basis of shear modulus. Elasticity wave equations are fairly complex, so that simplifying assumptions often must be made for standard MR elastography, where tissues are usually considered as linear, isotropic, homogeneous viscoelastic solids; compression and longitudinal waves are ignored (with respect to shear or transverse waves); and the wave propagation

Figure 7

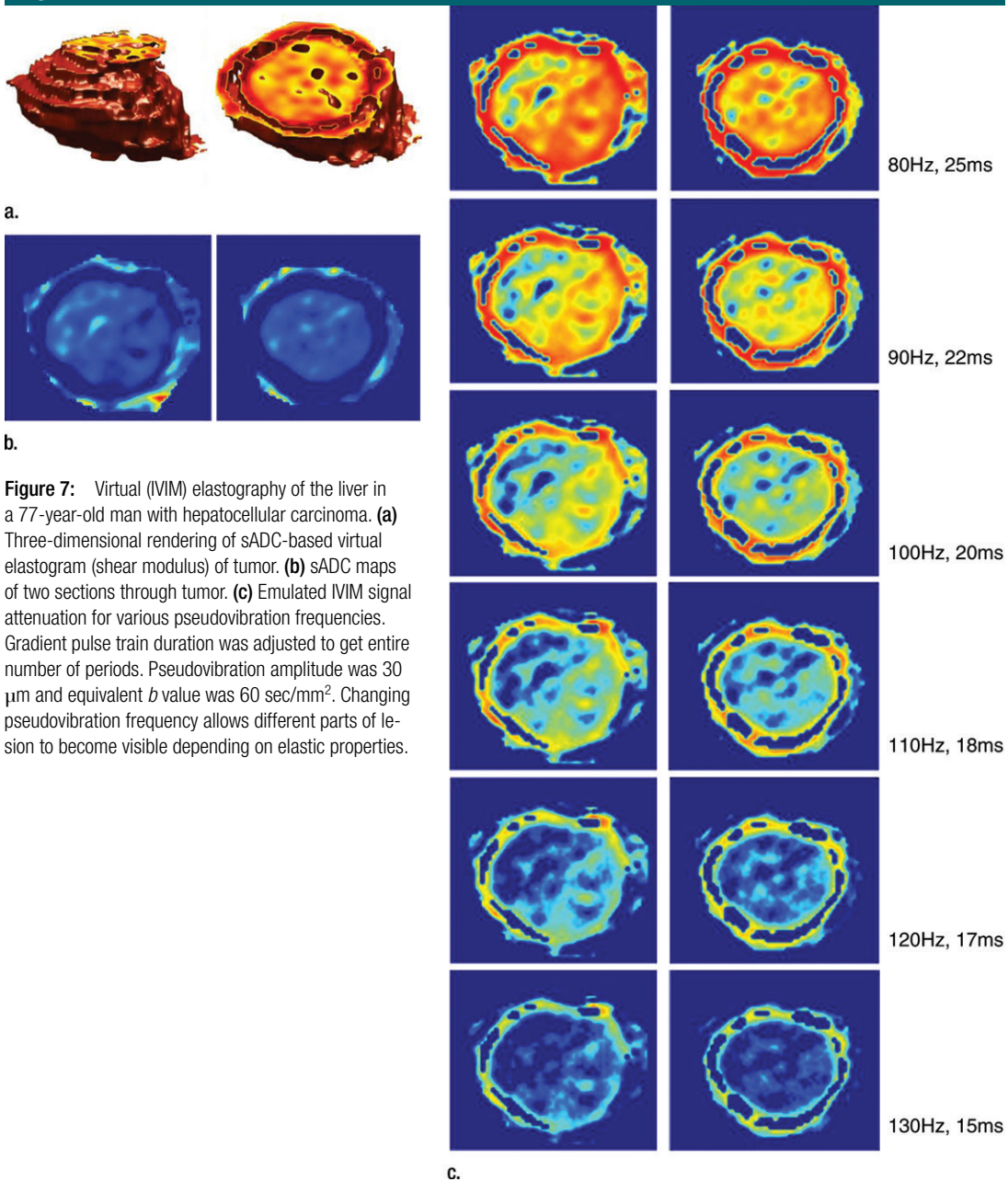

Figure 7: Virtual (IVIM) elastography of the liver in a 77-year-old man with hepatocellular carcinoma. **(a)** Three-dimensional rendering of sADC-based virtual elastogram (shear modulus) of tumor. **(b)** sADC maps of two sections through tumor. **(c)** Emulated IVIM signal attenuation for various pseudovibration frequencies. Gradient pulse train duration was adjusted to get entire number of periods. Pseudovibration amplitude was 30 μm and equivalent *b* value was 60 sec/mm^2. Changing pseudovibration frequency allows different parts of lesion to become visible depending on elastic properties.

direction and section orientation are assumed to coincide. The shear wave modulus is a complex valued quantity, and most often, only its magnitude is reported, although anisotropic, elastic, and viscous properties of tissues might be of interest (6). Although those quantities might be obtained from advanced MR elastographic techniques, further studies must be performed to investigate whether diffusion MR imaging or diffusion-tensor imaging in anisotropic tissues, probably through highly integrated tissue biomarkers such as the signature index (9), might provide similar information.

IVIM and diffusion MR imaging, through a suitable calibration of the $sADC_{200-1500}$ with standard MR elastography, can be quantitatively converted into elasticity shear modulus of the liver without using mechanical vibrations to potentially provide fibrosis staging. Virtual elastograms share the multisection and high resolution features from diffusion MR imaging. Propagating shear waves can also be

emulated, leading to a new elasticity-driven IVIM-like contrast for ranges of virtual vibration frequencies and amplitudes not limited by MR elastography or MR imaging hardware capacities.

Disclosures of Conflicts of Interest: D.L.B. Activities related to the present article: patent pending for MR imaging method. Activities not related to the present article: disclosed no relevant relationships. Other relationships: disclosed no relevant relationships. **S.I.** disclosed no relevant relationships. **U.M.** disclosed no relevant relationships.

References

1. Muthupillai R, Lomas DJ, Rossman PJ, Greenleaf JF, Manduca A, Ehman RL. Magnetic resonance elastography by direct visualization of propagating acoustic strain waves. Science 1995;269(5232):1854–1857.
2. Mariappan YK, Glaser KJ, Ehman RL. Magnetic resonance elastography: a review. Clin Anat 2010;23(5):497–511.
3. Singh S, Venkatesh SK, Wang Z, et al. Diagnostic performance of magnetic resonance elastography in staging liver fibrosis: a systematic review and meta-analysis of individual participant data. Clin Gastroenterol Hepatol 2015;13(3):440–451.e6.
4. Rousselet MC, Michalak S, Dupré F, et al. Sources of variability in histological scoring of chronic viral hepatitis. Hepatology 2005;41(2):257–264.
5. Srinivasa Babu A, Wells ML, Teytelboym OM, et al. Elastography in chronic liver disease: modalities, techniques, limitations, and future directions. RadioGraphics 2016;36(7):1987–2006.
6. Manduca A, Oliphant TE, Dresner MA, et al. Magnetic resonance elastography: non-invasive mapping of tissue elasticity. Med Image Anal 2001;5(4):237–254.
7. Le Bihan D, Breton E, Lallemand D, Aubin ML, Vignaud J, Laval-Jeantet M. Separation of diffusion and perfusion in intravoxel incoherent motion MR imaging. Radiology 1988;168(2):497–505.
8. Le Bihan D. Apparent diffusion coefficient and beyond: what diffusion MR imaging can tell us about tissue structure. Radiology 2013;268(2):318–322.
9. Iima M, Le Bihan D. Clinical intravoxel incoherent motion and diffusion MR imaging: past, present, and future. Radiology 2016;278(1):13–32.
10. Ichikawa S, Motosugi U, Morisaka H, et al. MRI-based staging of hepatic fibrosis: Comparison of intravoxel incoherent motion diffusion-weighted imaging with magnetic resonance elastography. J Magn Reson Imaging 2015;42(1):204–210.
11. Jiang T, Tian G, Zhao Q, et al. Diagnostic accuracy of 2D-shear wave elastography for liver fibrosis severity: a meta-analysis. PLoS One 2016;11(6):e0157219.
12. Leitão HS, Doblas S, Garteiser P, et al. Hepatic fibrosis, inflammation, and steatosis: influence on the MR viscoelastic and diffusion parameters in patients with chronic liver disease. Radiology 2017;283(1):98–107.
13. Yin Z, Magin RL, Klatt D. Simultaneous MR elastography and diffusion acquisitions: diffusion-MRE (dMRE). Magn Reson Med 2014;71(5):1682–1688.
14. Ishak K, Baptista A, Bianchi L, et al. Histological grading and staging of chronic hepatitis. J Hepatol 1995;22(6):696–699.
15. Rouvière O, Yin M, Dresner MA, et al. MR elastography of the liver: preliminary results. Radiology 2006;240(2):440–448.
16. Chabert S, Meca C, Le Bihan D. Relevance of the information about the diffusion distribution in vivo given by kurtosis in q-space imaging [abstr]. In: Proceedings of the Twelfth Meeting of the International Society for Magnetic Resonance in Medicine. Berkeley, Calif: International Society for Magnetic Resonance in Medicine, 2004; 1238.
17. Jensen JH, Helpern JA, Ramani A, Lu H, Kaczynski K. Diffusional kurtosis imaging: the quantification of non-gaussian water diffusion by means of magnetic resonance imaging. Magn Reson Med 2005;53(6):1432–1440.
18. Alkalay RN, Burstein D, Westin CF, Meier D, Hackney DB. MR diffusion is sensitive to mechanical loading in human intervertebral disks ex vivo. J Magn Reson Imaging 2015;41(3):654–664.
19. Taouli B, Chouli M, Martin AJ, Qayyum A, Coakley FV, Vilgrain V. Chronic hepatitis: role of diffusion-weighted imaging and diffusion tensor imaging for the diagnosis of liver fibrosis and inflammation. J Magn Reson Imaging 2008;28(1):89–95.
20. Bonekamp S, Torbenson MS, Kamel IR. Diffusion-weighted magnetic resonance imaging for the staging of liver fibrosis. J Clin Gastroenterol 2011;45(10):885–892.
21. Wang QB, Zhu H, Liu HL, Zhang B. Performance of magnetic resonance elastography and diffusion-weighted imaging for the staging of hepatic fibrosis: A meta-analysis. Hepatology 2012;56(1):239–247.
22. Glaser KJ, Felmlee JP, Manduca A, Ehman RL. Shear stiffness estimation using intravoxel phase dispersion in magnetic resonance elastography. Magn Reson Med 2003;50(6):1256–1265.